Escola de Primavera de Transição e Turbulência
Blumenau 2020

ABCM Associação Brasileira de Engenharia e Ciências Mecânicas

12th Spring School on Transition and Turbulence
September 21st-25th, 2020, Blumenau, SC, Brazil

EPTT-2020-0026
NUMERICAL EVALUATION OF MULTIPHASE FLOW IN A PILOT-SCALE THERMOSIPHON: A PRELIMINARY VALIDATION STUDY

Bruna Iten Bittelbrunn
University of Blumenau – São Paulo St. 3250, Blumenau – SC
brunaiten@gmail.com

Harlley Henrique Parno
University of Blumenau – São Paulo St. 3250, Blumenau – SC
hparno@gmail.com

Roberto Fischer Junior
University of Blumenau – São Paulo St. 3250, Blumenau – SC
robertofischerjr@gmail.com

Eduardo Oliveira
Petróleo Brasileiro S.A. – Petrobras – RJ-116, km 5,2, access A-1, Itaboraí – RJ
eduardooliveira@petrobras.com.br

Celso Murilo dos Santos
University of Blumenau – São Paulo St. 3250, Blumenau – SC
celsomurilo@gmail.com

Waldir Pedro Martignoni
University of Blumenau – São Paulo St. 3250, Blumenau – SC
wpmartignoni@yahoo.com.br

Henry França Meier
University of Blumenau – São Paulo St. 3250, Blumenau – SC
meier@furb.br

Jaci Carlo Schramm Câmara Bastos
University of Blumenau – São Paulo St. 3250, Blumenau – SC
camarabastos@gmail.com

Abstract. *Thermosiphons, also known as natural circulation loops, are heat transfer devices in which the fluid flows due to temperature gradient, generating single-phase and multiphase flow. In this study, a simplification of a pilot-scale thermosiphon was numerically evaluated. Volume of Fluid (VOF) with Lee model for mass transfer and Euler-Euler with RPI model simulations were conducted. The results were compared with an experimental database obtained by Particle Image Velocimetry (PIV) and Phase Doppler Anemometry (PDA) measurements. The results showed a qualitative agreement with the use of RPI model. However, further research is still needed to obtain a quantitative validation.*

Keywords: *pilot-scale thermosiphon, nucleate boiling, multiphase flow.*

1. INTRODUCTION

Thermosiphons are heat transfer devices which operate based on natural circulation phenomenon. Due to temperature difference, the fluid flows generating single-phase and multiphase flow (Zhang et al., 2015). As heat is given to the system, fluid temperature rises. On single-phase applications, the heat added to the system generates a density difference, which is the driving force to natural circulation. For multiphase flows, the fluid evaporates, generating a multiphase turbulent regime with heat and mass transfer. Moreover, bubble presence influences fluid flow. Due to its relatively simple project and working principles, thermosiphons are widely applied in industrial plants (Franco and Filippeschi, 2012). As cooling devices, thermosiphons can be found in small-scale applications such as electronic equipment (Woei, Feng and Yuan, 2011) and in large-scale application as nuclear reactor cooling system (Angelo et al., 2012). For heating

applications, thermosiphons are widely found as solar energy systems (Aung and Li, 2013) and vapor generators (Martinelli Júnior, 1998).

To comprehend and predict the behavior of thermosiphon systems, experimental and numerical investigations have been commonly performed in the literature. Krepper and Rzehak (2011) validated an Eulerian-Eulerian model for high pressure conditions using RPI model for heat transfer. DEBORA experiments were used as a comparison. These experiments were conducted by Garnier, Manon, and Cubizolles (2001) in a tube with 19 mm internal diameter and dichlorofluoromethane as working fluid in order to emulate the extreme conditions of nuclear reactors' cooling systems. The authors collected data regarding vapor volumetric fraction, vapor phase velocity, and bubble diameter using optical probes, and temperature data using thermocouples. Regarding numerical results, Krepper and Rzehak (2011) emphasized that some parameters such as bubble detachment diameter and nucleation site density needed recalibration.

Colombo and Fairweather (2016) studied the accuracy of an Eulerian-Eulerian two-fluid model on predicting subcooled boiling. The model included the RPI model for heat flux and a populational balance approach for bubble diameter distribution. Numerical results were compared with a large database, including the works of Bartolomej and Chanturiya (1967) and the DEBORA experiments. In the work of Bartolomej and Chanturiya (1967), an experimental unit was proposed to evaluate volumetric fraction and temperature profiles for an upward water flow in a 15.4 mm internal diameter and 2 m length heated tube. Different pressures, mass flows, and heat fluxes were evaluated resulting in a complete experimental database. Quantitatively, Colombo and Fairweather (2016) model's prediction was found satisfactory in terms of void fraction and liquid temperature. The authors affirmed that a model capable of including different experimental conditions was still needed.

More recently, Lee et al. (2019) conducted an experimental and numerical investigation of a vertical flow subcooled boiling regime. The experimental apparatus consisted in a 2.5 mm by 5 mm rectangular channel with a 114.6 mm heated length, where heat was provided from two opposite walls. A 2D computational simulation was conducted with Volume of Fluid (VOF) approach and Lee's phase change model (Lee, 1980). The authors claimed that the numerical model presented a strong capability to predict and represent boiling flow. Although, it was also affirmed that a 2D domain limited the flow treatment.

Computational fluid dynamics (CFD) have been shown to be a valuable tool to predict and comprehend the behavior of thermosiphon systems. However, most validated models present restricted application to the systems in which they were tested. Besides, most experiments are conducted in small idealized experimental units, deviating from industrial designs. In this context, the aim of this paper is to numerically evaluate the heating section of a pilot-scale thermosiphon operating with constant heat flux to posteriorly validate with an experimental database. Therein, the section was assessed via numerical simulation with Euler-Euler approach and RPI model as boiling model and VOF approach and Lee model for mass transfer. The preliminary results were compared with liquid phase velocity and liquid rate data obtained by Particle Image Velocimetry (PIV) technique, and vapor rate data obtained by Phase Doppler Anemometry (PDA).

2. METHODOLOGY

2.1 Experimental methods

A pilot-scale experimental facility is available to the authors of this work to conduct experiments regarding boiling flow in thermosiphons. The loop is divided in five main parts, as shown in Fig. 1. The riser is divided in two subsections: a 0.5 m high evaporation section (a) where heat is given to a 40.2 mm internal diameter tube by four electrical resistances; and a 0.8 m high glass visualization section (b), where experimental measurements are conducted. The liquid-vapor separator (c) consists in a cylindrical steel reservoir with 200 mm internal diameter and 300 mm length, adding up to a volume of 10 L, destinated to allow only vapor to enter the condenser (d). Once condensed, water flows to the downcomer (e), which is made of glass and kept at a constant temperature to cool the working fluid.

Temperature data can be acquired in six points along the experimental unit. Wall temperature is measured in the riser heating section, and fluid temperature is measured in two points of the riser visualization section, one point of the liquid-vapor separator, and two points of the downcomer.

For validation purposes, a database of velocity profiles will be used. Velocity profiles were obtained by PIV technique. In the most conventional configuration, a plane laser pulse is emitted on a plane in the flow. The light is reflected by tracing particles and the first image is recorded by a Charged Coupled Device (CCD) camera. After a time interval, a second laser pulse is emitted, and a second image is recorded. Particles position in both images is compared. Based on the particles' displacement and time interval between the two pulses, flow velocity can be determined. In this work, CCD camera and laser were disposed perpendicular to each other. Measurement area was set 270 mm above the end of the riser heating section, as highlighted in Fig. 1. Titanium dioxide particles were used as tracer. Time between pulses was stablished at 0.01 s. All measurements were made in triplicate, and average values taken at 300 mm above the end of the riser heating section are reported. Acquisition and data processing were made at LaVision DAVIS 8.1 software.

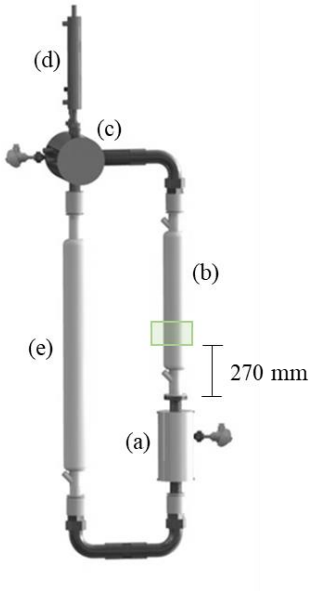

Figure 1. Thermosiphon unit divided in (a) riser heating section, (b) riser visualization section, (c) liquid-vapor separator, (d) condenser, and (e) downcomer.

For evaporation rate determination, an experimental database obtained by PDA technique was used. Data acquisition occurs with the emission of two laser beams. When a bubble passes through the interception of the two laser beams, light is dispersed. Reflected light is captured by an optical receptor and converted to a frequency proportional to bubble velocity. Besides, phase displacement between signals is a direct measure of bubble diameter. In this work, bubble velocity was used to determinate evaporation rate. Measurements were made at 300 mm above the end of the riser heating section.

Table 1 presents the heat flux imposed to the system as well as the experimental data obtained and therefore used for comparison with numerical results.

Table 1. Experimental conditions.

Condition	Value
Heat flux	24.97 W/m²
Experimental mean velocity	0.0316 ± 0.0018 m/s
Experimental temperature	95.7 ± 2.0 °C
Experimental liquid rate	0.0586 kg/s
Experimental vapor rate	$1.91 \cdot 10^{-7}$ kg/s

Preliminary measurements conducted with PIV allowed the comparison of numerical and experimental data regarding velocity profiles for the liquid phase and liquid rate. Results obtained using PDA technique allowed the analysis of evaporation rate. Thus, CFD simulations were conducted as a prior study for model validation.

2.2 Numerical methods

The thermosiphon domain in the simulation is presented in Fig. 2. It consisted in a simplification from the pilot-scale experimental unit to decrease computational effort and simulation time. The evaporation section was divided in the two subsections previously discussed. RPI and Lee models previously studied by Parno et. al (2019) were used to describe boiling phenomenon. This numerical study was conducted using the experimental conditions previously discussed in Bittelbrunn (2019). The author noticed a significant change in flow behavior due to the presence of a curve upstream the evaporation section. Thus, the computational domain was designed in a J-shaped form. All geometric characteristics were set as found in the pilot-scale experimental unit. Numerical grid can be seen in Figure 3.

The inlet boundary condition was set specifying a fixed pressure of 11610.75 Pa and a fixed temperature of 90°C. The pressure is equal to the water column in the pilot-scale unit and the temperature was obtained by experimental measures. At the evaporation section, a constant heat flux of 24.96 kW/m² was imposed. Visualization section was considered adiabatic since it is insulated at the pilot-scale unit. The outlet boundary condition was set as a static pressure of 0 Pa.

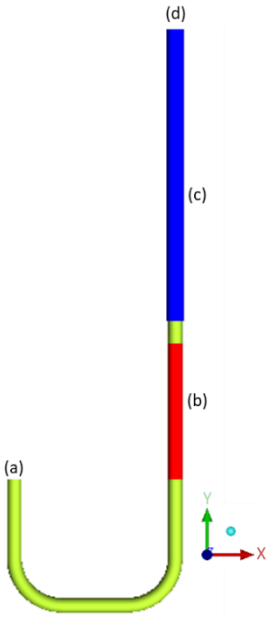

Figure 2. Computational domain, including (a) inlet, (b) heating section, (c) visualization section, and (d) outlet.

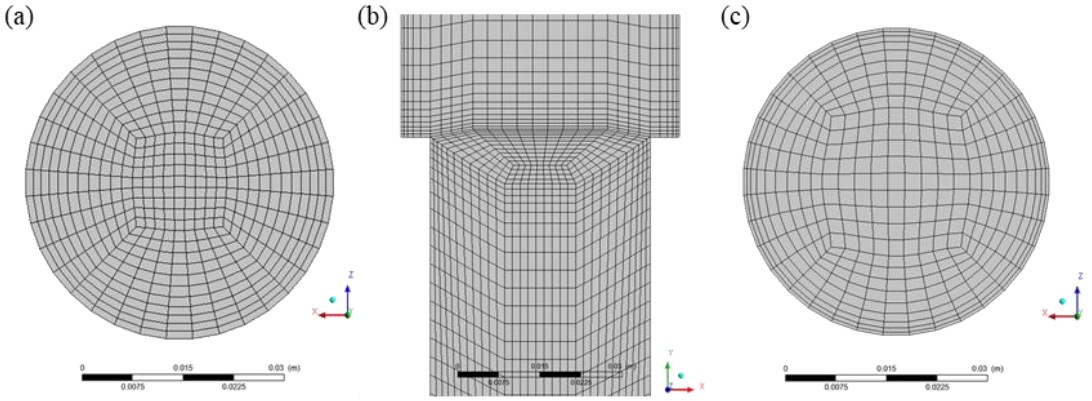

Figure 3. Numerical grid for (a) evaporation section, (b) transition between both sections, and (c) visualization section.

VOF approach by Hirt and Nichols (1981) was used to model the phases. In this approach, both fluids share the same transport equations. Thus, conservation equations for mass, momentum, and energy are described by Eq. (1), Eq. (2), and Eq. (3), respectively.

$$\frac{\partial \rho}{\partial t} + \boldsymbol{\nabla} \cdot (\rho \boldsymbol{v}) = 0 \tag{1}$$

where t is time, ρ is density, and $\boldsymbol{v}$ is the average velocity vector.

$$\frac{\partial}{\partial t}(\rho \boldsymbol{v}) + \boldsymbol{\nabla} \cdot (\rho \boldsymbol{v}\boldsymbol{v}) = -\nabla \mathrm{P} - \boldsymbol{\nabla} \cdot \mu_{eff}(\nabla \boldsymbol{v} + \nabla \boldsymbol{v}^T) + \rho \boldsymbol{g} \tag{2}$$

where P is the average static pressure and μ_{eff} is the effective viscosity.

$$\frac{\partial}{\partial t}(\rho E) + \boldsymbol{\nabla} \cdot [\boldsymbol{v}(\rho E + p)] = \boldsymbol{\nabla} \cdot \left(k_{eff} \nabla \mathrm{T}\right) + S_h \tag{3}$$

where E stands for energy, which is calculated by Eq. (4), T is the temperature, k_{eff} is the effective thermal conductivity, and S_h is the source therm.

$$E = \frac{\sum_{q=1}^{n} \alpha_q \rho_q E_q}{\sum_{q=1}^{n} \alpha_q \rho_q} \tag{4}$$

where E_q is based on the specific heat of each phase and the shared temperature. The volumetric fraction for phase q is represented by α_q. If there is only fluid q in the computational cell, then α_q equals one. If there is no fluid q in the cell, then α_q equals zero. If there is an interface between two fluids in the cell, then α_q is between zero and one.

For turbulence modelling, k-ω SST model was used, as previously studied by Guerra (2017). Mass transfer between both phases was modelled by the Lee model. Equation (5) describes mass transfer from the liquid to the vapor phase (Lee, 1980).

$$M_{lv} = c \cdot X_k \cdot \rho_l \cdot \frac{T_l - T_{sat}}{T_{sat}} \tag{5}$$

In Eq. (5) the subscribed letters l and v stand for liquid and vapor, respectively, X_k is the volumetric fraction for phase k, T_{sat} represents the saturation temperature, and c is a constant regarding interfacial mass transfer adjusted based on experimental data. In this work, the value of c was varied in three levels between 0.001 and 0.01.

Additionally, a two-fluid Eulerian-Eulerian approach was adopted to describe the flow. Conservation equations for mass, momentum, and energy for liquid and vapor phases are showed in Eq. (6) to Eq. (11), respectively.

$$\frac{\partial}{\partial t}(f_l \rho_l) + \nabla \cdot (f_l \rho_l \mathbf{v}_l) = M_{lv}^{+} - M_{vl}^{+} \tag{6}$$

$$\frac{\partial}{\partial t}(f_v \rho_v) + \nabla \cdot (f_v \rho_v \mathbf{v}_v) = M_{vl}^{+} - M_{lv}^{+} \tag{7}$$

$$\frac{\partial}{\partial t}(f_l \rho_l \mathbf{v}_l) + \nabla \cdot (f_l \rho_l \mathbf{v}_l \mathbf{v}_l) = -f_l \nabla P - \nabla \cdot \left[f_l (\boldsymbol{\tau}_l - \boldsymbol{\tau}_l^T)\right] + M_{lv}^{+} \mathbf{v}_v - M_{vl}^{+} \mathbf{v}_l + \mathbf{F}_{lv} + (f_l \rho_l \mathbf{g}) \tag{8}$$

$$\frac{\partial}{\partial t}(f_v \rho_v \mathbf{v}_v) + \nabla \cdot (f_v \rho_v \mathbf{v}_v \mathbf{v}_v) = -f_v \nabla P - \nabla \cdot f_v \boldsymbol{\tau}_v + M_{vl}^{+} \mathbf{v}_l - M_{lv}^{+} \mathbf{v}_v + \mathbf{F}_{vl} + (f_v \rho_v \mathbf{g}) \tag{9}$$

$$\frac{\partial}{\partial t}(f_l \rho_l h_l) + \nabla \cdot (f_l \rho_l \mathbf{v}_l h_l) = \nabla \cdot \left(f_l \lambda_l^{ef} \nabla T_l\right) + Q_l^{lv} + M_{lv}^{+} h_{vs} - M_{vl}^{+} h_{ls} \tag{10}$$

$$\frac{\partial}{\partial t}(f_v \rho_v h_v) + \nabla \cdot (f_v \rho_v \mathbf{v}_v h_v) = \nabla \cdot (f_v \lambda_v \nabla T_v) Q_v^{lv} + M_{vl}^{+} h_{ls} - M_{lv}^{+} h_{vs} \tag{11}$$

where $\boldsymbol{\tau}$ is stress tensor, λ is the thermal conductive coefficient, Q is the volumetric rate of heat transfer, M is the volumetric rate of mass transfer, and h stands for enthalpy.

The RPI wall boiling model was used to describe the wall heat flux based on the partitioned heat flux hypothesis. Equations (12) to (14) describe the heat given to the system by convective, evaporative, and quenching heat fluxes, respectively.

$$q_C'' = h_C (T_W - T_L)(1 - A_b) \tag{12}$$

$$q_E'' = V_d N_A \rho_g h_{fg} f_B \tag{13}$$

$$q_Q'' = \frac{2\sqrt{k_l \rho_l C_{p,l} f_B}}{\sqrt{\pi}} (T_W - T_L) \tag{14}$$

where the subscribed letters W and L stand for wall and liquid, respectively, A_b is the fraction of total area where there is bubble formation, V_d is the bubble volume, N_A is active sites density, f_B is bubble departure frequency, and $C_{p,l}$ is the liquid heat capacity. Equation (13) provides the portion of heat flux destinated to evaporation and describes mass transfer between phases, seen in the transport equations.

All stages of the simulation were conducted in ANSYS® commercial software. Transient simulations were conducted with a variable time step (global Courant number equals to 1) and a residual convergence criterion of 10^{-3}. Averages were acquired for 120 s after simulation stabilization. All numerical analyses were made at the plane where experimental data was obtained by PIV and PDA measurements and points where temperature data was obtained with thermocouples.

3. RESULTS AND DISCUSSIONS

Simulations were conducted with RPI and Lee models. In the first, a Euler-Euler approach was used with compressible model for the interface. In the latter, VOF method was used along with geometry reconstruction for the interface. Difference between cases regarding the interfacial mass transfer coefficient can be seen in Table 2. Values were estimated based on previous tests. For Lee model, only evaporation was considered as a mass transfer mechanism. For RPI model,

the constant was set for evaporation effects. The effect that interfacial mass transfer coefficient change caused in the evaporation and liquid rates is also shown in Tab. 2. Errors were calculated based on the experimental results of 0.0586 kg/s for liquid rate and $1.91 \cdot 10^{-7}$ kg/s for evaporation rate (Bittelbrunn, 2019).

Table 2. Effect of interfacial mass transfer constant change.

Case	Model	Interfacial mass transfer constant	Liquid rate (kg/s)	Error (%)	Evaporation rate (kg/s)	Error (%)
Case 1	VOF/Lee	0,0010	0.029	50.51	$1,07 \cdot 10^{-7}$	43.98
Case 2	VOF/Lee	0,0050	0.042	28.33	$1,59 \cdot 10^{-7}$	16.75
Case 3	VOF/Lee	0,0100	0.083	41.64	$9,82 \cdot 10^{-8}$	48.59
Case 4	Euler/RPI	0,0010	0.123	109.90	$5,59 \cdot 10^{-7}$	192.67
Case 5	Euler/RPI	0,0050	0.063	7.51	$3,50 \cdot 10^{-8}$	81.67
Case 6	Euler/RPI	0,0100	0.050	14.68	$4,68 \cdot 10^{-9}$	97.55

For Lee model, vapor generation is proportional to the interfacial mass transfer coefficient. Vapor formation also depends on the volumetric fraction presented in the computational cell and the difference between the calculated and the saturation temperatures. For RPI model, condensation also occurs since the model describes subcooled boiling. Thus, interfacial mass transfer works as a proportional factor, when 1 represents the complete condensation of the vapor phase and 0 represents no condensation. For both models, the interfacial mass transfer coefficient works as a weighting factor and must be calibrated based on experimental results.

Differences between cases showed that the two models behave differently when predicting the boiling phenomenon. Lee model estimates vapor generation based on fluid temperature, which is estimated by the transport equations. On the other hand, RPI model is based on the partition of the heat flux, set as boundary condition. So, vapor generation is estimated by the portion of the heat flux destinated to phase change. Essentially, evaporation rate depends directly on the value set for the interfacial mass transfer coefficient. As seen in Tab. 2, when the liquid rate obtained in numerical simulations agreed with the experimental result, evaporation rate was subpredicted. For liquid rate, a better agreement was found for RPI simulations. However, for evaporation rate, Lee model presented a better prediction. Quantitatively, neither Lee nor RPI model presented a good agreement.

For a qualitative analysis, Figure 4 presents the velocity profile for the liquid phase obtained by PIV measurements. Then, Figure 5 presents the comparison between numerical and experimental data regarding the velocity profile of the liquid phase when numerical cases were conducted with Lee model. Both measurements were made 300 mm above the end of the evaporation section. Tube radius is presented in its dimensionless form.

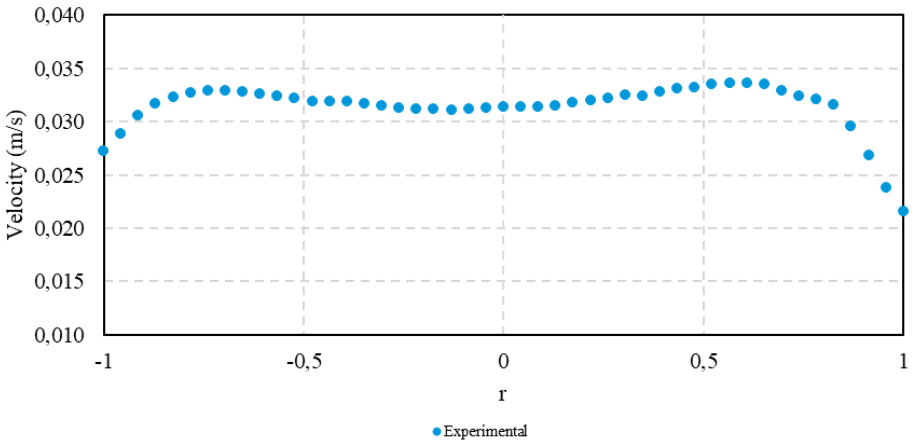

Figure 4. Experimental velocity profile for the liquid phase.

From Figure 4, higher velocities can be found closer to the tubes' walls. When compared to numerical data from Lee model, as seen in Figure 5, a deviation can be seen. The model predicted higher velocities near the left side of the tube, decreasing when approaching the right side. Also, velocities were mostly overpredicted.

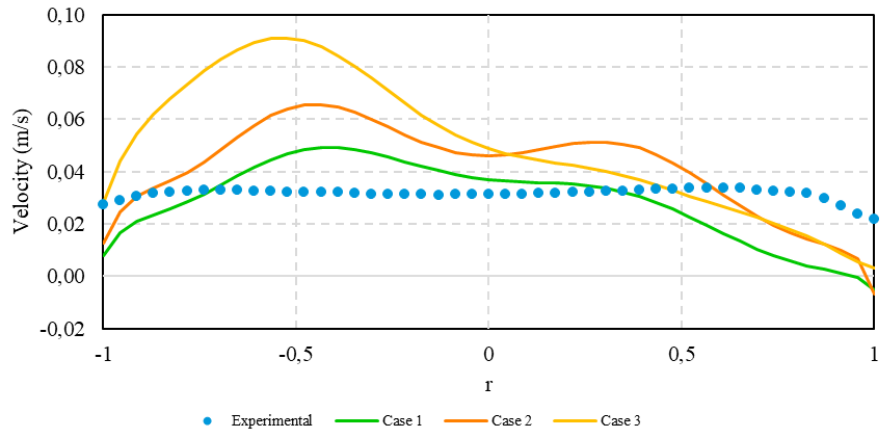

Figure 5. Comparison between experimental and numerical velocity profiles for the liquid phase with Lee model.

Figure 6 presents the comparison between numerical and experimental data regarding the velocity profile of the liquid phase when numerical cases were conducted with RPI model.

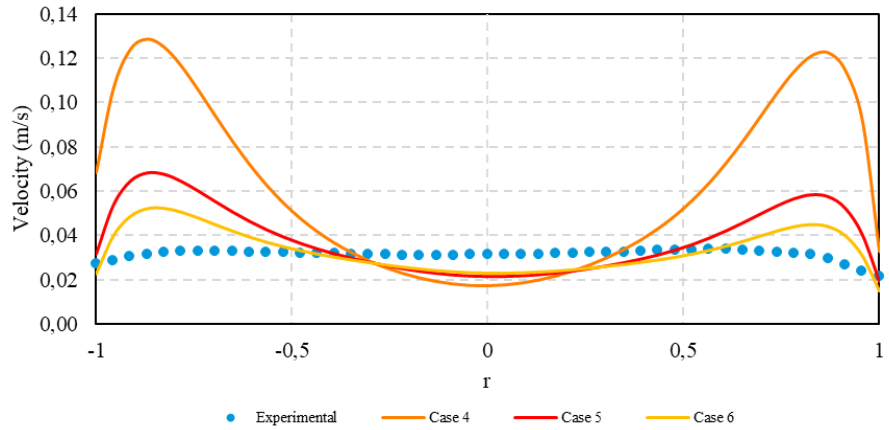

Figure 6. Comparison between numerical and experimental velocity profiles for the liquid phase with RPI model.

The comparison between numerical and experimental velocity profiles showed that the RPI model was able to qualitatively predict the behavior of liquid phase velocity profile. The peaks of higher velocities near walls were captured by the model. For showing a better agreement, a comparison between experimental data and numerical data from Case 6 is presented in Figure 7.

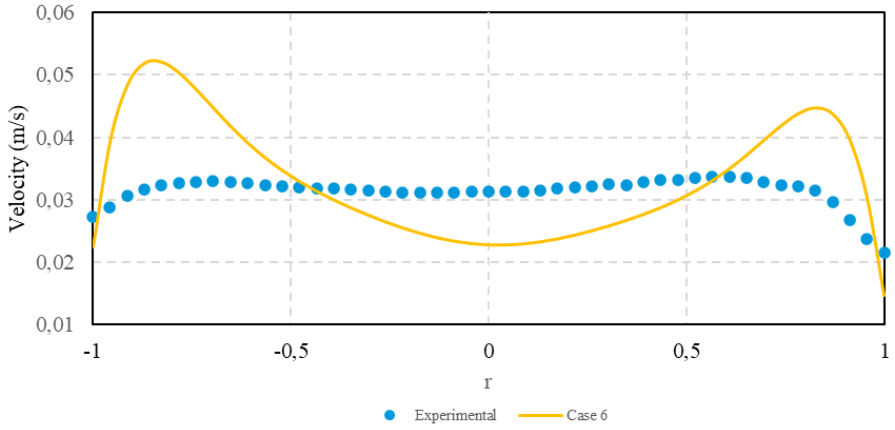

Figure 7. Comparison between Case 6 and experimental velocity profiles for the liquid phase.

Developed multiphase boiling flow tend to present this velocity profile pattern, with lower velocities at the center of the tube and higher velocities near walls (Lee, Park, and Lee, 2002). The alteration seen on the right peak of both velocity profiles showed in Figure 7 is a consequence of the flow alteration caused by the curve upstream the evaporation section. The plane where data were acquired is less than 20 diameters away from the curve, which implicates in a non-developed flow (Abdulkadir et al., 2015). The similarity between experimental and numerical profiles, also regarding this alteration, shows that the RPI model is better suited for the continuity of this validation work.

Quantitative validation was not achieved due to the simplification of the numerical domain. When the geometry was simplified to a J-shaped form, pressure drops occurring in other locations of the loop were ignored. Therefore, numerical velocity profile would only agree with experimental data if the vapor rate were subpredicted. Contrarily, when the vapor rate agreed with experimental data, the velocity profile was overpredicted. To correct this discrepancy, future research will be conducted considering the complete geometry of the experimental unit.

Regarding temperature measurements, Table 3 presents the mean temperatures of the fluid, from numerical and experimental measurements.

Table 3. Experimental and numerical results for fluid temperature (°C).

Case	Heating section outlet temperature
Experimental	97.50
Case 1	97.85
Case 2	95.38
Case 3	92.82
Case 4	91.26
Case 5	94.20
Case 6	95.39

As presented in Table 3, temperature numerical data showed a good agreement, with a maximum 6.40% deviation from experimental results. For Case 6, a deviation of 2.16% was obtained. It is important to highlight that downcomer inlet temperature was set as a boundary condition for numerical simulations based on experimental measurements. Besides, the experimental value of 97.50°C is a local measurement obtained with a thermocouple positioned above the end of the riser heating section.

4. CONCLUSIONS

This preliminary study was conducted to evaluate both RPI and Lee model ability to predict subcooled nucleate boiling flow in a natural circulation loop. Therefore, a simplification of the experimental unit available for the authors was numerically simulated. Two models were tested, being the RPI model for an Euler-Euler approach and the Lee model for a VOF approach.

Both models can be used to simulate subcooled boiling flows. However, results for RPI model showed a better qualitative agreement with experimental data obtained by PIV and PDA measurements. RPI model was able to capture peaks of higher velocities showed in the experimental database. Nonetheless, velocity data was mostly overpredicted and a quantitative validation is still needed. In this regard, further research is being conducted considering the complete geometry, to include effects such as pressure drops caused by flow reversions.

5. ACKNOWLEDGEMENTS

The authors are grateful for the financial support of PETROBRAS for this research project, through the cooperation agreement number 5850.0103010.16.9, and CNPq through Process 308714/2016-4.

6. REFERENCES

Abdulkadir, M., Hernandez-Perez, V., Lo, S., Lowndes, I.S. and Azzopardi, B.J., 2015. “Comparison of experimental and Computational Fluid Dunamics (CFD) studies of slug flow in a vertical riser”. *Experimental Thermal and Fluid Science*, Vol. 68, p. 468-483.

Angelo, G., Andrade, D.A., Angelo, E., Torres, W.M., Sabundjian, G., Macedo, L.A. and Silva, A.F., 2012. “A numerical and three-dimensional analysis of steady state rectangular natural circulation loop”. *Nuclear Engineering and Design*, Vol. 244, p. 61–72.

Aung, N., Li, S., 2013. “Numerical investigation on effect of riser diameter and inclination on system parameters in a two-phase closed loop thermosyphon solar water heater”. *Energy Conversion and Management*, Vol. 75, p. 25–35.

Bartolomej, G.G. and Chanturiya, V.M., 1967. “Experimental study of true void fraction when boiling subcooled water in vetical tubes”. *Thermal Engineering*, Vol. 14, p. 123-128.

Bittelbrunn, B.I., 2019. *Análise experimental do escoamento multifásico com ebulição nucleada em um termossifão projetado por simulação numérica*. Master dissertation, University of Blumenau, Blumenau.

Colombo, M. and Fairweather, M., 2016. "Accuracy of Eulerian-Eulerian, two-fluid CFD boiling models of subcooled boiling flows". *International Journal of Heat and Mass Transfer*, Vol. 103, p. 28–44.

Franco, A. and Filippeschi, S., 2012. "Closed loop two-phase thermosyphon of small dimensions: A review of the experimental results". *Microgravity Sci. Technol*, Vol. 24, p. 165-179.

Garnier, J., Manon, E. and Cubizolles, G., 2011. "Local measurements on flow boiling of refrigerant 2 in a vertical tube". *Multiphase Science and Technology*, Vol. 13, p. 1–111.

Guerra, H., 2017. *Escoamento multifásico com ebulição nucleada em sistema de circulação natural.* Master dissertation, University of Blumenau, Blumenau.

Hirt, C.W. and Nichols, B.D., 1981. "Volume of fluid (VOF) method for the dynamics of free boundaries". *Journal of Computational Physics*, Vol. 39, p. 1043-1044.

Krepper, E. and Rzehak, R., 2011. "CFD for subcooled flow boiling: Simulation of DEBORA experiments". *Nuclear Engineering and Design*, Vol. 241, p. 3851-3866.

Lee, J., O'Neill, L.E., Lee, D. and Mudawar, I., 2019. "Experimental and computational investigation on two-phase flow and heat transfer of highly subcooled flow boiling in vertical upflow". *International Journal of Heat and Mass Transfer*, Vol. 136, p. 1199–1216.

Lee, T.H., Park, G.C.and Lee, D.J., 2002. "Local flow characteristics of subcooled boiling flow of water in a vertical concentric annulus". *International Journal of Multiphase Flow*, Vol. 28, p. 1351–1368.

Lee, W.H., 1980. "A pressure iteration scheme for two-phase flow modeling". *Multiphase Transport: Fundamentals, Reactor Safety, Applications*, p. 407-432.

Martinelli Júnior, L.C., 1998. *Geradores De Vapor*. Panambi, Rio Grande do Sul.

Parno, H.H., Bittelbrunn, B.I., Fischer Jr., R., dos Santos, C.M., Bastos, J.C.S.C. and Meier, H.F., 2019. "Comparação entre modelos de ebulição no *riser* de um termossifão". In *Proceedings of the IV Simpósio Paranaense de Modelagem, Simulação e Controle de Processos.* Curitiba, Brazil.

Woei, S., Feng, K., Yuan, C., 2011. "Loop thermosyphon electronic cooling device operated at sub-atmospheric pressure". In: *10th International Heat Pipe Symposium*, p. 158–166, 2011.

Zhang, P., Wang, B., Shi, W. and Li, X., 2015. "Experimental investigation on two-phase thermosyphon loop with partially liquid-filled downcomer". *Applied Energy,* Vol. 160, p. 10-17.

7. RESPONSIBILITY NOTICE

The authors are the only responsible for the printed material included in this paper.